CHAPTER 9

Computational investigation on the molecular interactions between MDM2 and its inhibitor XR-2

Computational investigation on the molecular interactions between MDM2 and its inhibitor XR-2

9.1. Abstract:

An essential negative regulator of the tumour suppressor p53 molecule is the MDM2 protein. Thus, inhibiting the interaction between MDM2 and p53 molecules is necessary to regulate the p53 activity. Recently, a small molecule with the chemical name 2-(2-(2-methoxyethoxy)ethoxy)ethyl-(29S,3R,49S,59R)-5'-((4-carbamoyl-2-methoxyphenyl)carbamoyl)-6-chloro-4'-(3-chloro-2-fluorophenyl)-29-neopentyl-2-oxospiro[indoline-3,39-pyrrolidine]-19-carboxylate (also called XR-2) was found to bind to the NTD of MDM2, resulting in reactivation of functioning of p53 molecules. In this study, we have studied the interaction profile as well as the structural dynamics of MDM2-XR-2 complex using molecular dynamics simulation. It was found that XR-2 remained intact within the N-Terminal binding cavity of MDM2 throughout the simulation. We also carried out the BFE as well as PRED analyses for the MDM2-XR-2 complex. The binding affinity was found to be good ($\Delta G_{binding}$ = -16.26 kcal mol^{-1}), and residues PHE55, ILE61, VAL93 and LEU58 of MDM2 provide the highest energy contributions for the interaction between MDM2 and XR-2.

9.2. Introduction:

About 50% of all human malignancies include mutations in the tumor-suppressor protein p53. A near universal mutation (96%) in serous ovarian cancer and a rare occurrence (10%) in thyroid cancer are both examples of p53 mutations, which are more common in some cancer types than others [691]. This discrepancy offers therapeutic potential for targeting p53 wild-type (WT) tumours in a different way than p53 mutant tumours [692, 693]. The reconfiguration of mutant p53 to its active, normal WT conformation restores apoptosis and induces tumour regression, according to a number of preclinical studies [694, 695].

The fast destruction of p53 by the proteasome ensures that intracellular levels of p53 are kept low under normal circumstances. This degradation can be influenced by a variety of signalling pathways, including sumoylation, phosphorylation, acetylation, methylation, and glycosylation. It can occur in both ubiquitin-dependent [676] and

ubiquitin-independent [696] modes [697]. The most significant of them is ubiquitination [698, 699], and the E3 ligase MDM2 is the main inhibitor of p53 [700, 701], while there are also a number of additional E3 and E4 ligases of p53. The N-terminal of MDM2 interacts with the p53 N-terminal TAD, which promotes its C-terminal RING finger E3 ligase activity and allows ubiquitin to be transferred to several lysine residues in p53's core DNA-binding and C-terminal regulatory domains [698, 699]. The transcriptional activity of p53 is adversely influenced by MDM2 ubiquitination (either mono- or poly-ubiquitination). Nuclear export is triggered by mono-ubiquitin, while nuclear p53 is targeted by poly-ubiquitin for proteasome breakdown [702]. Additionally, p53 up-regulates MDM2 transcriptionally, and this negative feedback loop, along with cyclical control of both proteins' levels, ensures that p53 levels are kept low under normal circumstances.

A recently synthesized chemical compound: 2-(2-(2-methoxyethoxy)ethoxy)ethyl-(29S,3R,49S,59R)-5’-((4-carbamoyl-2-methoxyphenyl)carbamoyl)-6-chloro-4’-(3-chloro-2-fluorophenyl)-29-neopentyl-2-oxospiro[indoline-3,39-pyrrolidine]-19-carboxylate (also called XR-2) was found to interact with the MDM2(NTD) [703].

In the present study, we have investigated the conformational dynamics and stability, as well as the interaction profile of the MDM2-XR-2 complex. We also carried out BFE and PRED analyses to infer the binding characteristics and identify hotspot residues across the interface of MDM2(NTD) in the MDM2-XR-2 complex.

9.3. Materials & Methods:

9.3.1. Preparation of the MDM2(NTD)-XR-2 system:

The 3-D structure of MDM2 bound to the TAD1 of p53 protein (PDB ID: 1YCR) was obtained from the RCSB PDB. The structure was then visualized using the UCSF Chimera software v.1.13.1 and the MDM2 protein from the MDM2-p53 complex was separated and was saved as a new file.

The 3D structure of the small molecule XR-2 was constructed using MolView server. The small molecule XR-2 was then visualised using the ArgusLab visualization software v.4.0.1, followed by its energy optimization by the UFF (universal force field).

The PatchDock web server was then used to prepare the MDM2-XR-2 complex.

The best docked model was chosen based on section based on the principle mentioned in section **7.3.1**.

9.3.2. MD simulation of the MDM2(NTD)-XR-2 system:

The MD simulation study on the MDM2-XR-2 complex was then performed using the Assisted Model Building with Energy Refinement (AMBER) 14 software package, where ff99SB force field parameters were used for the protein part of the system, while the ligand (XR-2) was treated with the generalized AMBER force field (GAFF) parameters. The rest of the steps were performed as mention in section **7.3.2**.

9.3.3. Analysis of the MD Trajectories:

The analysis of the MD trajectories have been performed using the modules mentioned in section **4.3.3**.

9.3.4. Secondary Structure comparison of the MDM2(NTD)-XR-2 Complex:

Using the RMSD clustering algorithm, the lowest energy conformer for the complex taken from the highly populated clusters. The lowest energy conformer was then submitted to the 2Struc online server to study the secondary structural components of MDM2 in MDM2-XR-2 complex.

9.3.5. BFE and PRED analyses of the MDM2(NTD)-XR-2 Complex:

The BFE and the PRED of the MDM2-XR-2 complex interface residues analyses were carried out using the procedure mentioned in section **4.3.6.**

9.4. Results & Discussions:

9.4.1. Analysis of the conformational changes of the MDM2(NTD)-XR-2 Complex:

We have performed MD simulation on the MDM2(NTD)-XR-2 complex. After equilibration, the complex was subjected to production dynamics for 50 ns (**Figure 9.1**). From **Figure 9.1**, it can be observed that XR-2 remains bound to the N-Terminal binding cavity of MDM2 throughout the simulation.

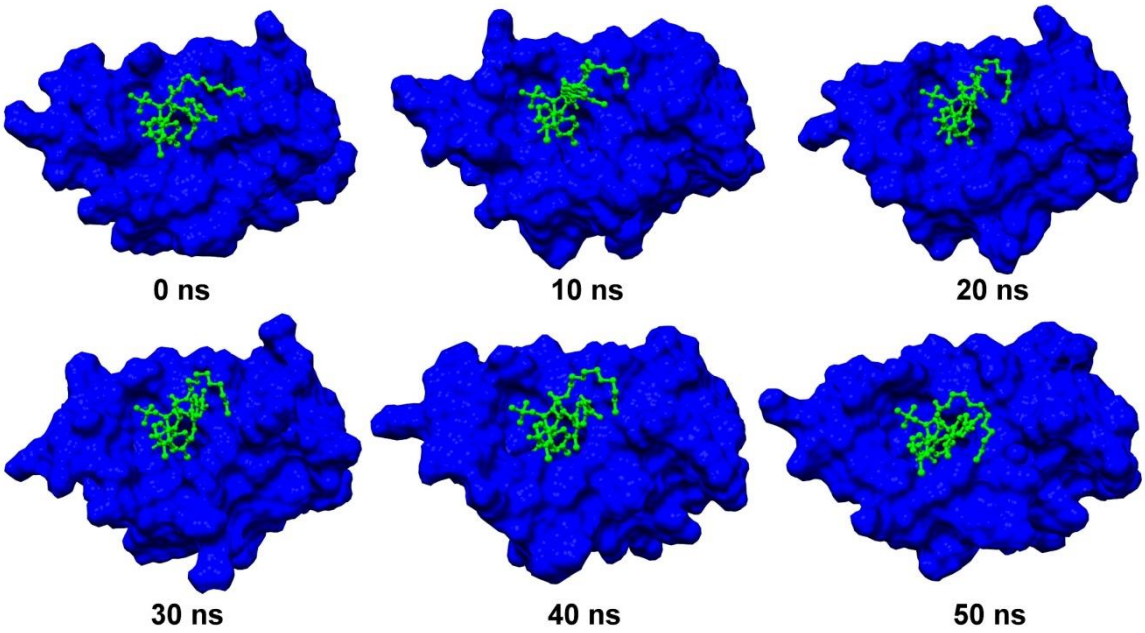

Figure 9.1. *Conformations of MDM2-XR-2 at different time intervals of simulation.*

9.4.2. LigPlot analysis of the various conformers of the MDM2(NTD)-XR-2 Complex obtained during the MD simulation:

The structures of the complex extracted at different intervals of MD simulation were then subjected to LigPlot analysis to obtain the protein ligand interaction profiles. It was found that almost the same residues from MDM2(NTD) were interacting with XR-2 at different intervals of the simulation (**Figure 9.2**).

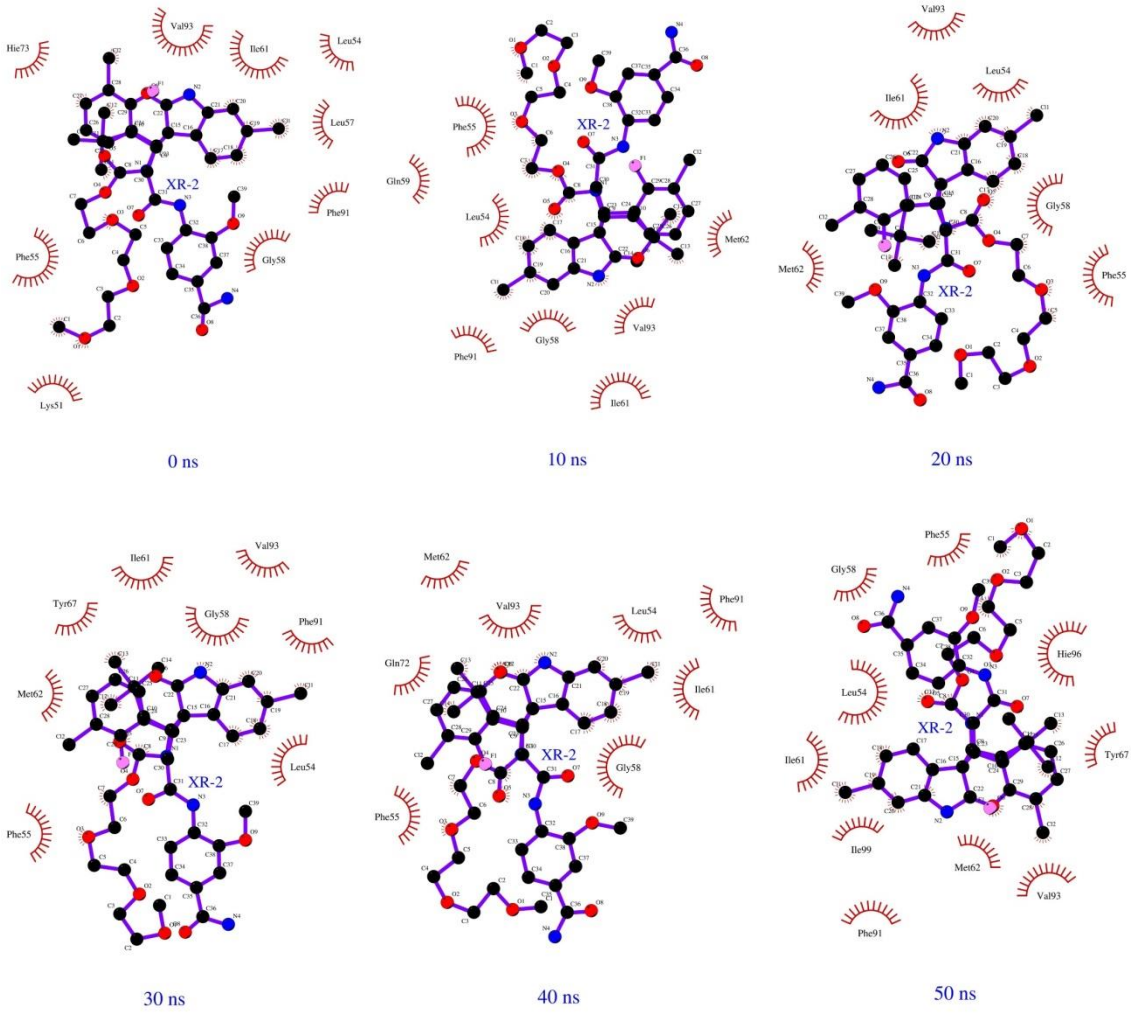

Figure 9.2. *LigPlot analysis of MDM2-XR-2 at different time intervals of simulation.*

Various structural properties such as RMSD, RMSF, Rg, SASA, number of intermolecular hydrogen bonds, and the secondary structural elements were evaluated separately for MDM2-XR-2 complex.

9.4.3. RMSD analysis of the MDM2(NTD)-XR-2 Complex:

The RMSD graph was plotted for Cα atoms for the complex as shown in **Figure 9.3**. We observed RMSD oscillate till 7.5 ns of simulation time and then found settled for the rest of the simulation time. The average RMSD value of MDM2-XR-2 complex was found to be 1.5 Å.

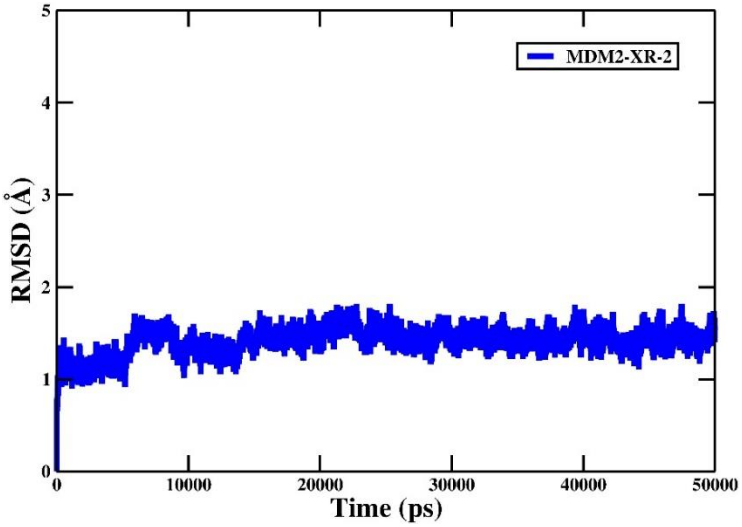

Figure 9.3. *RMSD analysis of MDM2-XR-2 complex.*

9.4.4. RMSF analysis of the MDM2(NTD)-XR-2 Complex:

Then we determined the Residue flexibility in the MDM2-XR-2 complex using RMSF analysis. **Figure 9.4** shows the RMSF values for C-α atoms of the complex. From the RMSF plot, we see fluctuation of C-α atoms in the residue numbers: 18-20, 42-45, and in the extreme N-Terminal and C-Terminal residues of MDM2.

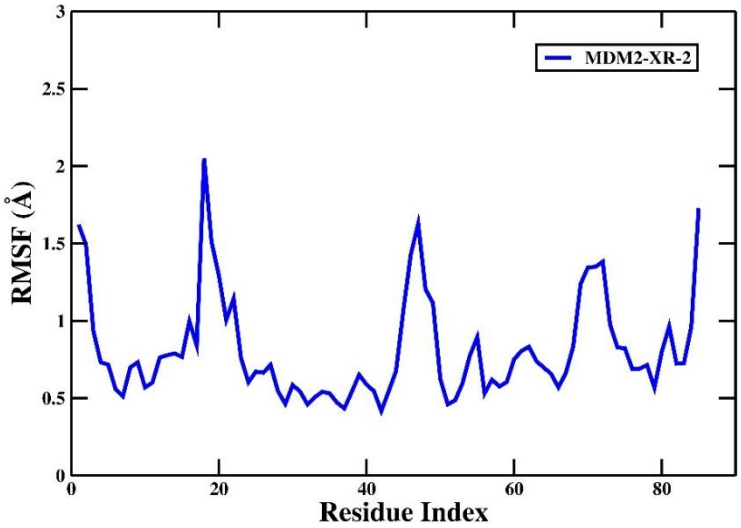

Figure 9.4. *RMSF analysis of MDM2-XR-2 complex.*

9.4.5. Rg analysis of the MDM2(NTD)-XR-2 Complex:

Rg is another important geometrical parameter, which indicates the compactness of a system over a period of simulation time. For a protein molecule to be stable, it should

maintain its compactness in an optimal temperature and pressure conditions. The average Rg values for the MDM2-XR-2 complex was found to be 13 Å, which remained constant throughout the simulation (**Figure 9.5**).

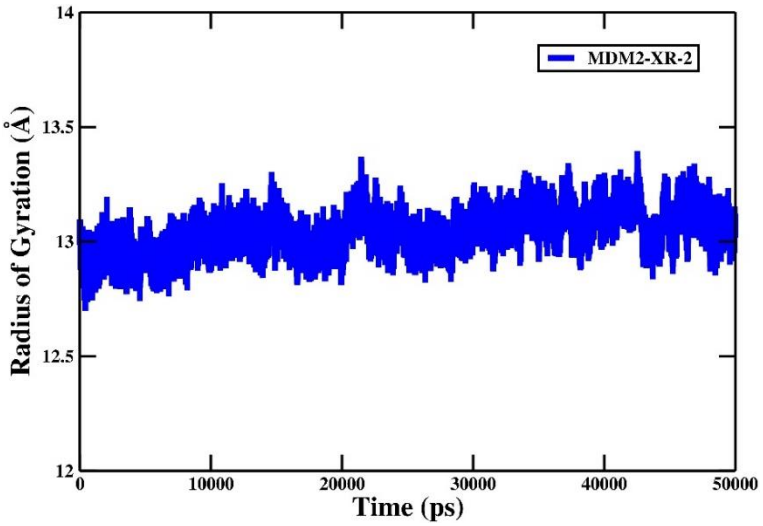

Figure 9.5. *Rg analysis of MDM2-XR-2 complex.*

9.4.6. SASA analysis of the MDM2(NTD)-XR-2 Complex:

The SASA gives an overview of the behavior of residues with respect to solvent, and determines the stability of the protein. The SASA for MDM2-XR-2 complex was calculated to be 5800 $Å^2$ (**Figure 9.6**).

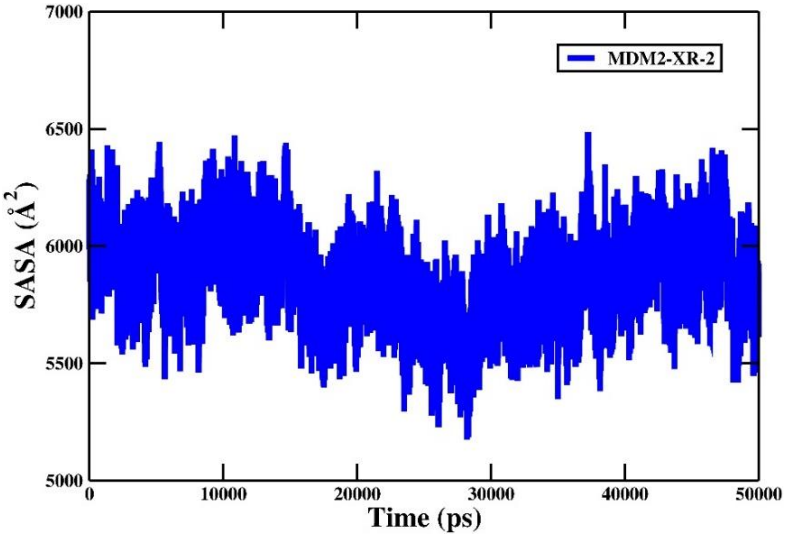

Figure 9.6. *SASA analysis of MDM2-XR-2 complex.*

9.4.7. Hydrogen bond analysis of the MDM2(NTD)-XR-2 Complex:

Additionally, we also carried out the analysis of inter-molecular hydrogen bonds present

in the MDM2-XR-2 complex. The number of hydrogen bonds was observed to be within the ideal range as proposed for the globular proteins. **Figure 9.7** represents the intermolecular hydrogen bond analysis of the complex. The average number of intermolecular hydrogen bonds in the complex with MDM2(NTD) as donor and XR-2 as acceptor was found to be 2, and with XR-2 as donor and MDM2(NTD) as acceptor was also found to be 2.

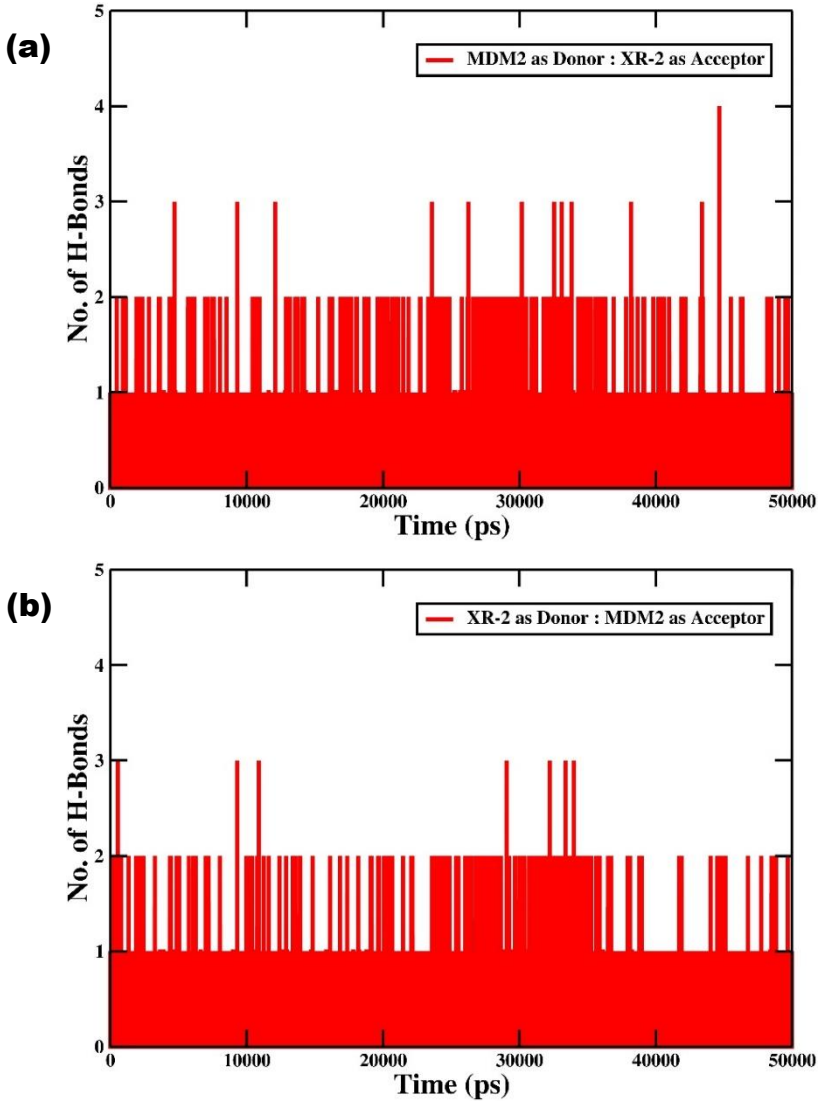

Figure 9.7. *Inter-molecular hydrogen bond analysis of MDM2-XR-2complex with (a) MDM2 as Donor and XR-2 as acceptor; and (b) XR-2 as Donor and MDM2 as acceptor.*

9.4.8. Analysis of probable secondary structure per residue of MDM2(NTD) in the MDM2(NTD)-XR-2 Complex:

Then we carried out the analysis of the probable secondary structure that each residue of

MDM2 can adopt in MDM2-XR-2 complex (**Figure 9.8**). From **Figure 9.8,** we infer that the MDM2 molecule contains the secondary structure α-helix predominantly in the regions 7-20, 25-40, 56-65, and 70 -82 residues.

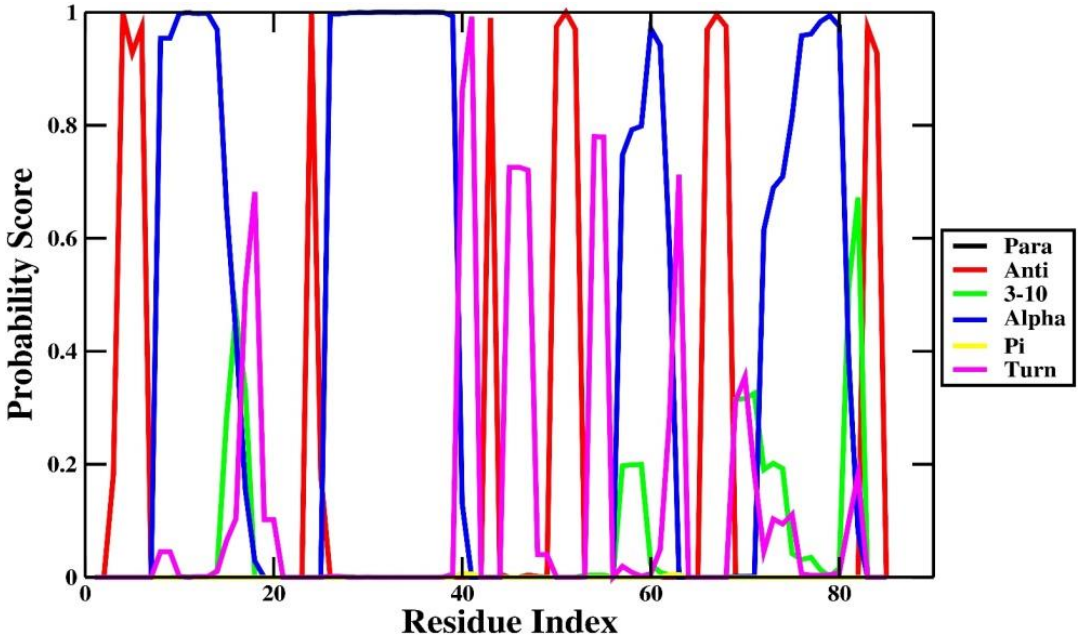

Figure 9.8. *Probability score for secondary structure analysis of MDM2 in the MDM2-XR-2 complex.*

9.4.9. DSSP analysis of MDM2(NTD) in the MDM2(NTD)-XR-2 Complex:

Then we performed the DSSP analysis using the Kabsch and Sander algorithm to investigate the changes in secondary structural elements in the MDM2 molecule (as shown in **Figure 9.9**). From **Figure 9.9**, it can be observed that a good amount of the α/3_{10}-helix and anti-parallel beta sheets to be present in MDM2 throughout the simulation.

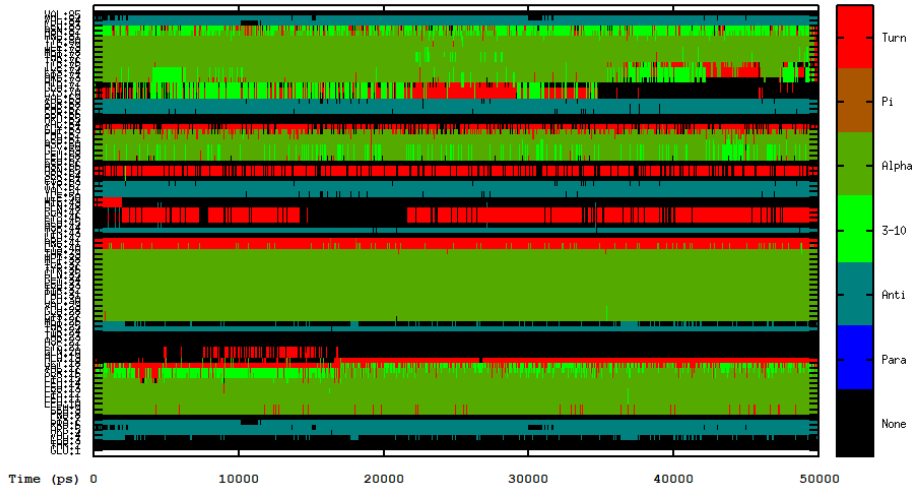

Figure 9.9. *The evolution of secondary structure evaluated using DSSP is shown for MDM2 molecule in MDM2-XR-2 complex.*

9.4.10. Secondary Structure comparison of the MDM2(NTD)-XR-2 Complex with the p53(TAD1)-MDM2(NTD) complex (PDB ID:1YCR):

In addition, the secondary structure content of MDM2 present in the lowest energy structure of the MDM2-XR-2 complex extracted using RMSD clustering algorithm, and the p53(TAD1)-MDM2(NTD) complex have been calculated using the 2StrucCompare server (**Table 9.1**), it was found that MDM2 present in the MDM2-XR-2 complex has 41.2% helices, while MDM2 present in the p53(TAD1)-MDM2(NTD) complex has 34.9% helices.

Table 9.1. *Secondary structure analysis of the lowest energy structure of MDM2-XR-2 complex and p53-MDM2 complex (PDB ID: 1YCR) using 2Struc online server.*

	α-Helix (%)	***3_{10}-Helix (%)***	***Turns (%)***
MDM2-XR-2	*41.2*	*0*	*15.3*
p53-MDM2	*34.9*	*0*	*11.9*

9.4.11. BFE and PRED analyses of the MDM2(NTD)-XR-2 Complex:

The BFE calculations of MDM2 and XR-2 to form the MDM2-XR-2 complex were performed using the MM-GBSA method, a module of the AMBER14 software package.

The BFE evaluated for the MDM2-idasanutlin complex, together with the descriptions of the energy terms, are shown in **Table 9.2**. From **Table 9.2**, all the derived components required for the BFE analysis have been observed to contribute to the binding of MDM2 and idasanutlin to form the MDM2-idasanutlin complex. The total BFE ($\Delta G_{binding}$) was found to be -16.26 kcal mol $^{-1}$, which indicates a good binding affinity between MDM2 and XR-2 molecule in the MDM2-XR-2 complex.

Table 9.2. *The various components of the Binding Free Energy (kcal mol^{-1}) evaluated by MM/GBSA method between MDM2-XR-2 complex.*

Components	**Complex (kcal mol^{-1})**	**Standard Deviation (±)**	**Receptor (kcal mol^{-1})**	**Standard Deviation (±)**	**Ligand(kcal mol^{-1})**	**Standard Deviation (±)**	**$\Delta\Delta G_{bind}$ (kcal mol^{-1})**	**Standard Deviation (±)**
$\Delta E_{VDWAALS}$	-699.92	11.3102	-637.58	10.62	-20.69	2.21	-41.65	2.82
ΔE_{EL}	-6114.35	29.54	-6022.26	29.53	-91.9	2.77	-0.19	3.48
ΔE_{GB}	-1252.14	19.84	-1226.06	20.17	-38.80	1.48	12.72	3.58
ΔE_{SURF}	41.50	0.811	39.97	0.74	6.51	0.18	-4.98	0.33
ΔG_{gas}	-842.03	34.36	-851.68	35.21	51.48	6.85	-41.83	4.60
ΔG_{solv}	-1210.64	62.19	-1186.09	19.91	-32.29	1.48	7.74	3.45
ΔG_{TOTAL}	-13842.54	19.57	-2037.77	25.65	19.20	6.60	**-34.09**	2.73
TS_{TRA}	16.00	0	15.9272	0	13.68	0	-13.62	0
TS_{ROT}	15.84	0	15.79	0	11.84	0.02	-11.79	0.02
TS_{VIB}	1074.59	1.93	1000.001	1.64	67.00	0.89	7.58	3.03
TS_{TOTAL}	1106.42	1.93	1031.72	1.64	92.53	0.91	**-17.83**	3.05
$\Delta G_{binding}$							**-16.26**	

ΔE_{EL} = electrostatic energy as calculated by the MM force field; **$\Delta E_{VDWAALS}$** = van der Waals contribution from MM; **ΔE_{GB}** = the electrostatic contribution to the polar solvation free energy calculated by GB; **ΔE_{SURF}** = non-polar contribution to the solvation free energy calculated by an empirical model; **ΔG_{gas}** = total gas phase energy (**ΔG_{gas}** = **ΔE_{EL}** +**$\Delta E_{VDWAALS}$**);**ΔG_{solv}** = sum of nonpolar and polar contributions to solvation; **ΔG_{TOTAL}** = final estimated binding free energy in kcal mol^{-1} calculated from the terms above (**ΔG_{TOTAL}** = **ΔG_{gas}** +**ΔG_{solv}**); **TS_{TRA}** = translational energy; **TS_{ROT}** = rotational energy; **TS_{VIB}** = vibrational energy; **TS_{TOTAL}** = total entropic contribution; and **$\Delta G_{binding}$** = BFE.

To have an insight into the influence of each of the amino acid residues of MDM2 on the overall MDM2-XR-2 interaction, PRED values were determined implying the MM-GBSA method. **Figure 9.10** represents the PRED analysis for the interface residues of MDM2 present in the MDM2-XR-2 complex. The highest energy contribution can be observed from the residue PHE55, followed by residues ILE61, VAL93 and LEU54 of

MDM2 respectively.

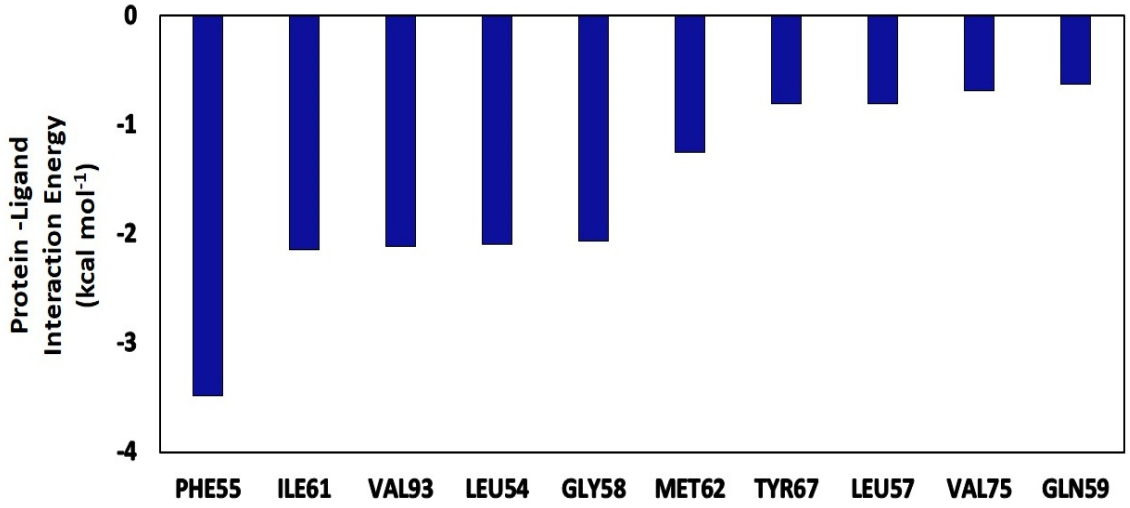

Figure 9.10. *Per Residue Energy Decomposition (PRED) analysis of MDM2 in MDM2(NTD)-XR-2 complex.*

9.5. Conclusion:

Here in this study, we have demonstrated the molecular interactions between MDM2 and its inhibitor XR-2. The small molecule XR-2 remains bound to the N-Terminal binding cavity of MDM2 throughout the simulation. The RMSD value for the MDM2-XR-2 complex is quite low (1.5 Å) and it remains constant throughout the simulation, which infers a very good stability between MDM2 and XR-2. There exists a good binding affinity between MDM2 and XR-2 was ($\Delta G_{binding}$ = -16.26 kcal mol^{-1}). The residues PHE55, ILE61, VAL93 and LEU58 of MDM2 provide the highest energy contributions for the interaction between MDM2 and XR-2. Our study's findings may be applied to the development of stronger MDM2 inhibitors, which would increase the effectiveness of cancer chemotherapy.